King Saud University

Arabian Journal of Chemistry

www.ksu.edu.sa
www.sciencedirect.com

ORIGINAL ARTICLE

Efficiency of a novel nitrogen-doped Fe$_3$O$_4$ impregnated biochar (N/Fe$_3$O$_4$@BC) for arsenic (III and V) removal from aqueous solution: Insight into mechanistic understanding and reusability potential

Hamid Ali [a], Saeed Ahmed [b], Abdelghani Hsini [c,d], Simon Kizito [e], Yassine Naciri [f], Ridha Djellabi [g], Muhammad Abid [h], Waseem Raza [i], Noor Hassan [j], Muhammad Saif Ur Rehman [k], Asif Jamal Khan [l], Muhammad Khan [m], Muhammad Zia Ul Haq [n], Dominic Aboagye [g], Muhammad Kashif Irshad [o], Munawar Hassan [p], Asif Hayat [q,r], Bo. Wu [a,s,*], Abdul Qadeer [t,*], Zeeshan Ajmal [u,*]

[a] *Multiscale Computational Materials Facility, Key Laboratory of Eco-Materials Advanced Technology, College of Materials Science and Engineering, Fuzhou University, Fuzhou 350100, China*
[b] *Department of Chemistry, University of Chakwal, Pakistan*
[c] *National Higher School of Chemistry (NHSC), University Ibn Tofail, BP. 133-14000, Kenitra, Morocco*
[d] *Laboratory of Advanced Materials and Process Engineering (LAMPE), Faculty of Science, Ibn Tofail University, BP 133, 14000, Kenitra, Morocco*
[e] *College of Agricultural and Environmental Sciences, Makerere University, Uganda*
[f] *Laboratoire Matériaux et Environnement LME, Faculté des Sciences, Université Ibn Zohr, BP 8106, Cité Dakhla, Agadir, Morocco*
[g] *Department of Chemical Engineering, Universitat Rovira i Virgili, 43007, Tarragona, Spain*
[h] *Department of Ocean Science and Engineering, Southern University of Science and Technology, Shenzhen, China*
[i] *Institute for Advanced Study, Shenzhen University, Shenzhen, Guangdong 518060, China*
[j] *School of Chemistry and Chemical Engineering, Beijing Institute of Technology, Beijing 100081, China*
[k] *Department of Chemical Engineering, Khwaja Fareed University of Engineering and Information Technology, Rahim Yar Khan 64200, Pakistan*
[l] *Shaanxi Key Laboratory of Earth Surface System and Environmental Carrying Capacity, College of Urban and Environmental Sciences, Northwest University, Xian, Shaanxi 710127, China*

* Corresponding authors.
E-mail addresses: wubo@fzu.edu.cn (Bo. Wu), Dr.AQ.Geographer@gmail.com (A. Qadeer), zeeshan@nwpu.edu.cn (Z. Ajmal), .
Peer review under responsibility of King Saud University.

[m] *School of Material Science and Engineering, Northwestern Polytechnical University, 71002, Xian, China*

[n] *Department of Agronomy, University of Agriculture, Faisalabad 38000, Pakistan*

[o] *Department of Environmental Sciences & Engineering, Government College University Faisalabad, Pakistan*

[p] *College of Economics and Management, Jilin Agricultural University Changchun, Jilin, China*

[q] *College of Chemistry and Life Sciences, Zhejiang Normal University, Jinhua 321004, Zhejiang, China*

[r] *College of Geography and Environmental Sciences, Zhejiang Normal University, Jinhua 321004, China*

[s] *Materials Design and Manufacture Simulation Facility, School of Advance Manufacturing, Fuzhou University, Jinjiang 362200, China*

[t] *National Engineering Laboratory for Lake Pollution Control and Ecological Restoration, Chinese Research Academy of Environmental Sciences, 10012, Beijing, China*

[u] *School of Chemistry and Chemical Engineering, Northwestern Polytechnical University, Xian, China*

Abstract   Worldwide, arsenic contamination has become a matter of extreme importance owing to its potential toxic, carcinogenic and mutagenic impact on human health and the environment. The magnetite-loaded biochar has received increasing attention for the removal of arsenic (As) in contaminated water and soil. The present study reports a facile synthesis, characterization and adsorption characteristics of a novel magnetite impregnated nitrogen-doped hybrid biochar (N/Fe_3O_4@BC) for efficient arsenate, As(V) and arsenite, As(III) removal from aqueous environment. The as-synthesized material (N/Fe_3O_4@BC) characterization via XRD, BET, FTIR, SEM/EDS clearly revealed magnetite (Fe_3O_4) impregnation onto biochar matrix. Furthermore, the adsorbent (N/Fe_3O_4@BC) selectivity results showed that such a combination plays an important role in targeted molecule removal from aqueous environments and compensates for the reduced surface area. The maximum monolayer adsorption (Q_{max}) of developed adsorbent (N/Fe_3O_4@BC) (18.15 mg/g and 9.87 mg/g) was significantly higher than that of pristine biochar (BC) (9.89 & 8.12 mg/g) and magnetite nano-particles (MNPs) [7.38 & 8.56 mg/g] for both As(III) and As(V), respectively. Isotherm and kinetic data were well fitted by Langmuir ($R^2 = 0.993$) and Pseudo first order model ($R^2 = 0.992$) thereby indicating physico-chemical sorption as a rate-limiting step. The co-anions (PO_4^{3-}) effect was more significant for both As(III) and As (V) removal owing to similar outer electronic structure. Mechanistic insights (pH and FTIR spectra) further demonstrated the remarkable contribution of surface groups (OH^-, $-NH_2$ and $-COOH$), electrostatic attraction (via H- bonds), surface complexation and ion exchange followed by external mass transfer diffusion and As(III) oxidation into As(V) by (N/Fe_3O_4@BC) reactive oxygen species. Moreover, successful desorption was achieved at varying rates up to 7th regeneration cycle thereby showing (N/Fe_3O_4@BC) potential practical application. Thus, this work provides a novel insight for the fabrication of novel magnetic biochar for As removal from contaminated water in natural, engineering and environmental settings.

1. Introduction

Toxic compounds such as heavy metal (loids) especially, arsenic (As) adversely affect to the human health and the natural environment mainly associated with its high toxicity, mutagenic and carcinogenic characteristics (Chakraborti et al., 2016; Qadeer et al., 2020; Essekri et al., 2022). Mineral weathering, geochemical reactions, mining, erosion, oil exploitation and As-bearing pesticides application have been reported as major source of groundwater As contamination (Gong et al., 2011). Depending upon pH and the redox potential, As contamination in water and soil can exist in different inorganic species such as; arsenite, As(III) and arsenate, As(V) and in organic form as; methylated As arsenocholine, and/or arsenobetaine (Urík et al., 2009; Zhang et al., 2017). In oxygen-rich environment (250–750 mV), the As (V) can exist in the form of $H_2AsO_4^-$, H_3AsO_4, $HAsO_4^{2-}$ and AsO_4^{3-}. Whereas, under oxygen-deficient environments (-250 to +250 mV), As(III) species are mainly dominant in the form of Arse-

nious acid (H_3AsO_3) at pH 1–9, which is in turn transformed into $H_2AsO_3^-$ as the solution pH approaches 12 at − 250 to − 500 mV redox (Kumarathilaka et al., 2018). To minimize its threshold level in an aquatic environment, many regulation authorities set an optimum threshold contaminant level of about 10 μg L^{-1} in drinking water (Fisher et al., 2015; Qadeer et al., 2022; Qadeer et al., 2022). In order to achieve low contamination level in water, several treatment strategies are employed including; coagulation, flocculation, photodegradation, ion exchange, chemical precipitation membrane filtration, and solvent extraction and adsorption (Yn et al., n.d.; Ff and Qi, 2011; Chen et al., 2019; Zhang and Jiang, 2019; Meng et al., 2020; Zhang et al., 2021; Ajmal et al., 2021; Hayat et al., 2022). These techniques are, however, associated with low adsorption/desorption capacities with high operational costs (Ajmal et al., 2020; Hayat et al., 2022; Brini et al., 2021). Notably, a positive bias towards adsorption technique is gaining more attention due to its high flexibility in design, ease in operation, and no sludge production and cost-effectiveness (Usman et al., 2018; He et al.,

2016). To this end, various adsorbents including magnetite nano-particles (Wang et al., 2010), surface modified biochar's (Ali et al., 2020; Ying et al., 2013), and granular activated carbon (Adeo et al., 2011) have been tested for the treatment of As contaminated water. Although the application of adsorption is somehow efficient, but the associated high cost most often limits their large-scale application (Ahmed et al., 2018; Khorram et al., 2016; Malik et al., 2021; Li et al., 2022). To minimize their high operational costs, the search for low cost, but highly efficient alternative sorbents is ongoing (Kizito et al., 2017; Wu et al., 2017; Ahmed et al., 2021; Hayat et al., 2022). The use of engineered surface adsorbents from agricultural-biomass has occupied a center stage by providing a low-cost alternative. Biochar (BC) is regarded as a potent raw material for making engineered adsorbent for aqueous separation processes (Hao et al., 2000; Kosik et al., 2020; Qadeer et al., 175 (2021)). In pristine form, the use of BC in aqueous separation is limited to its surface area, low contaminant specificity, and low end-process recovery (Naiya et al., 2009). After sorption, filtration and centrifugation steps are required for its efficient separation and irreversible sorption means that there are limited sorption sites to affect the second cycle contaminant removal. This phenomenon in turn limits the industrial scale BC application. However, to improve BC separation and species specificity during adsorption and regeneration (free of active sites) process, it's a prerequisite to modify and activate BC before being used as an effective adsorbent material (Bakouri et al., 2010; Pan et al., 2022).

For the case of As sorption, BC pretreatment or modification is an important step to increase sorption effectiveness and efficiency. In particular As(III) and As(V) adsorption capacities on pristine BC is generally known to be low owing to its more negative charge on its surface (Mudhoo et al., 2011). In literature, various BC modification techniques have already been employed to improve its porosity, functional groups, surface area and point of zero charge (pHpzc) (Jin et al., 2014). These strategies include, activation by alkaline/acidic solutions, impregnation with nanoparticles of iron (Fe) and nano zero valent metals and conjugation with functional groups such as amides and thiols (Tan et al., 2015). Most recently, modification of biochar with Magnetite (Fe_3O_4) is receiving incredible research attention owing to its structural Fe^{II} presence, high stability, more reactive surface sites, and good surface chemistry (Usman et al., 2013; Duan et al., 2018; Xi et al., 2021; Zhang et al., 2021). Furthermore, magnetic surface modification has been envisaged to offer a promising solution in terms of fast pollutant recovery associated with its high separation characteristics by applying external magnetic field. The use of magnetic biochar was encouraged to recover metal ions from contaminated water (Baokang et al., 2018). Moreover, for enhanced metal (loids) adsorption, nitrogen (N) doping has also been considered as a valuable aspect in sorption studies, mainly due to attracting anionic species (arsenic), but depending upon solution pH. The analysis of N doping could provide a highly positive charged sorption sites and ultimately enhance material adsorption characteristics towards anionic species (Yoo et al., 2018). For instance, the N-doped aquatic animal waste BC has already been reported for enhanced nickel (Ni) ions removal from contaminated water (Yin et al., 2019). The N-doping effect on corn straw derived BC for the adsorption of copper (Cu) and cadmium (Cd) was observed to be more significant (Usman et al., 2012). To the best of our knowledge, there exist enormous studies on N-doped BC to evaluate its effectiveness for the elimination of metal (loids) for aqueous solution (Chen et al., 2022; Wan et al., 2019; Wang et al., 2021).

However, there is no information available in order to draw a solid conclusion towards As(III) and As(V) removal from aqueous solution by using a Fe_3O_4 impregnated N-doped biochar. Thus, the main objective of the present study is: (i) to carry out the facile synthesis and characterization of magnetic ($N/Fe_3O_4@BC$) in order, (ii) to evaluate the sorption capacity (including the underlying mechanisms) for As(III) and As(V) from aqueous solutions, (iii) and evaluate its separation, regeneration and reuse in continuous sorption process. Furthermore, the mechanistic evaluation was also investigated by using different models and integration techniques. It is expected that this study would

prove a milestone for the ongoing research efforts for water purification from both engineering aspect and scientific approach under natural and environmental settings.

2. Experimental section

2.1. Material preparation and characterization

The preparation of magnetite nano-particles (MNPs) was carried out according to the procedure reported previously (Usman et al., 2012). The biochar preparation was carried out via slightly modified the method described earlier (Harikishore Kumar Reddy and Lee, 2014). Briefly, the wood pellets were cut into small pieces, and then transformed into powder form followed by washing and drying at 105 °C for 24 h. The magnetic biochar synthesis was carried out by immersing the as-obtained wood powder about 50 g by vigorous stirred (30 min) 500 mL solution of 9.25 g Ferric sulfate ($Fe_2(SO_4)_3 \cdot 9H_2O$) and 10 g of Iron(II) sulfate ($FeSO_4$). The solution pH was maintained in the range of (10–11) using 10 M sodium hydroxide (NaOH). Thereafter, the resultant mixture was dried at 65 °C followed by calcination at 550 °C for 150 min under nitrogen environment (Harikishore Kumar Reddy and Lee, 2014). A range of characterization techniques were used to determine the physico-chemical characteristics of the developed adsorbent. The Brunauer–Emmett–Teller (BET) surface area properties were investigated by using BELSORP MAX (BEL, Japan. Inc). The X-ray spectra by using Cu Kα radiation source were recorded on X-ray diffractometer (SHIMADZU XRD-6000). The scanning electron microscopic images were captured over (SEM, ZEISS SUPRA 55). The Fourier-transform infrared spectroscopy (FTIR) spectra were recorded within an intensity range of (400–4000 cm^{-1}) on FTIR measure equipment (FT-IR, Bruker Vector 22).

2.2. Batch experiments

Adsorption of As(III) and As(V) was evaluated by batch adsorption trials. Synthetic As(V) and As(III) stock solutions (1000 mg/L) were prepared through disodium hydrogen arsenate ($Na_2HAsO_4 \cdot 7H_2O$ Fluka, > 98 %) and sodium arsenite (Na_3AsO_4 Fluka, > 98 %). From the stock concentration, several dilutions (1–50 mg/L) were made. The solution pH was adjusted between 2 and 11 by using 0.1 M NaOH or HCl. The effect of different parameters on As(III & V) sorption was investigated by varying several parameters such as; reaction time was varied from 5 min to 24 h, the initial As concentration was varied from (1–35 mg/L), the phosphate concentration was varied from (1–6 mg/L), pH (2–11), and temperature (15–55 °C). The sorption vials were placed in water bath shaker at a constant agitation speed 150 rpm. At the end of each reaction time, about 5 mL of supernatant was collected and filtered through 0.45 µm syringe filter. The optimum adsorption capacity (mg/g) and removal (%) of As(V) was calculated after measuring residual adsorbate concentration of filtrate sample via molybdenum blue method as described by (Spectro molybdate method) at 880 nm (Dhar et al., 2004), via UV–vis spectrophotometer, and then, adsorption capacity on the basis of residual concentration was calculated through **Eqs.1** and **2**...$\frac{C_o - C_e}{C_o} \times 100$

$$Removal\% = \frac{C_o - C_e}{C_o} \times 100 \frac{C_o - C_e}{C_o} \times 100 \qquad (1)$$

$$q_e = \frac{C_o - C_e}{M} \times V \qquad (2)$$

where C_e and C_o are the final and initial metal ions concentrations (mg/L) in aqueous medium, q_e (mg/g) is the adsorbed amount per (g) of tested adsorbent, M represent the total adsorbent mass (g), while V is solution volume (L).

2.3. Desorption and regeneration tests

To investigate saturated particle regeneration potential for the developed adsorbent, the recovered particles were subject to several desorption/re-sorption trials using same pollutant concentrations and under similar conditions as those used with fresh particles. Desorption experiments were carried out by using deionized water and alkaline solutions. The adsorbate-loaded samples were centrifuged and the supernatant was decanted and discarded. Desorption was initiated by adding 10 mL of 0.1 M NaOH solution and agitated for 24 h. After agitation, the supernatant was filtered through 0.45-µm propylene syringe. Total desorbed concentration was measured through previously described adsorption estimation method. Prior to next adsorption experiments, the material was separated out, and oven dried (at 105 °C for 24 h). The dried particles were then used for subsequent adsorption/desorption/ regeneration analysis. The percentage (%) desorption performance was calculated through **Eq. (3)**:

$$Desorption\% = \frac{C * V}{X * m} \times 100 \frac{C_o - C_e}{C_o} \times 100 \qquad (3)$$

Where; C denotes desorbed metal ions concentration (mg/L), x is adsorbed capacity of metal ions prior to desorption (mg/g), m represents the total mass of particle, which is used in desorption analysis (g), while V denotes the desorption solution volume (L).

3. Results and discussion

3.1. Materials characterization

Characterization results showed that the surface area properties, like pristine BC surface area characteristics were found to be superior than magnetite modified biochar $Fe_3O_4@N/$ BC as shown in Table 1. Conversely, the lower porosity characteristics after magnetic modification are closely associated with the blockage of fine pores from iron species, which in turn led to the loss of micro-porosity (Kumar et al., 2014). Moreover, the decrease in surface area properties are due to the presence of higher proportion of iron layer over pristine BC

surface sites, and ultimately led to decline in surface area (Chen et al., 2011).

The variations in BC and ($N/Fe_3O_4@BC$) crystallographic structure were characterized by X-ray Powder Diffraction (XRD) Fig. 1a. A clear difference in XRD diffractograms of pristine BC and ($N/Fe_3O_4@BC$) was observed. A clear peak, especially at 30.19 A^o was observed for ($N/Fe_3O_4@BC$). According to Wang et al., (Wang et al., 2015), these new peaks onto $N/Fe_3O_4@BC$ were closely associated with the presence of Fe_3O_4. Moreover, the peaks at 42.13 A^o are an indication of cubic iron oxides particles over ($N/Fe_3O_4@BC$). The corresponding peaks at 57.43 A^o for ($N/Fe_3O_4@BC$), further indicates the occurrence of Fe_3O_4 (di-iron oxide, magnetite). The FTIR spectra were also recorded for MNPs, BC and Fig. 1b–d. Some new additional bands specifically at 501–585 cm^{-1} were observed for MNPs and BC, thereby indicating the presence of Fe–O surface functional group (Baig et al., 2014). Moreover, the basic proportion of K and Ca content, and Mg were considerably higher in pristine BC as compared to MNPs and ($N/Fe_3O_4@BC$). However, according to EDS spectra the contents of Fe were found higher in MNPs followed by ($N/Fe_3O_4@BC$) and BC.

The EDS spectra of $N/Fe_3O_4@BC$ also indicated a sharp line showing the existence of Fe impregnation into $N/Fe_3O_4@$ BC matrix shown in Fig. 2. Overall, all tested adsorbent surface sites were uniform in content, and containing a lot of irregular shaped material, as well as a wide range of undesirable particle aggregation **Figure. 1Sl**. In comparison, ($N/Fe_3O_4@BC$)exhibited lower carbon content, which obviously indicated that magnetic modification process results into the loss of organic matter contents Fig. 2 (Perlman et al., 267 (1992)).

3.2. Adsorption characteristics

3.2.1. Effect of as initial concentration

Optimum adsorption performance of tested materials is utterly associated with initial solution concentration since, it drives mass transfer rate underneath elevated concentration ranges between bulk liquid to solid interfaces (Auta and Hameed, 2013). The results of Fig. 3a & b, show the variation in solution concentration for As adsorption towards tested material surface sites within examined concentrations ranges (1–5 mg/L). The adsorption capacity (mg/g) and adsorption efficiency (%) indicated an entirely reverse order against elevated As solution concentration. From the Fig. 3a & b, it is clearly apparent that As(III, V) adsorption was increased by increasing initial solution concentration (1–35 mg/L) (C_o–C_e), while that of % removal was decreased. The maximum adsorption rate at highest concentration (35 mg/L) was observed to be 43.74 mg/g for As(III) and 23.69 mg/g for As(V) in (N/Fe_3-

Table 1 The physico-chemical properties of tested materials used in this study.

Adsorbent Sample	BET SSA (m^2/g)	Pore volume cm^3/g	Pore diameter (nm)	PZC
Magnetic biochar (N/Fe$_3$O$_4$@BC)	109.40	0.447	16.3	8.2
Biochar (BC)	123.07	0.442	38.8	7.7
Magnetite nano-particles (MNP$_S$)	72.20	0.411	23.0	7.1

SSA; specific surface area, PZC; point of zero charge.
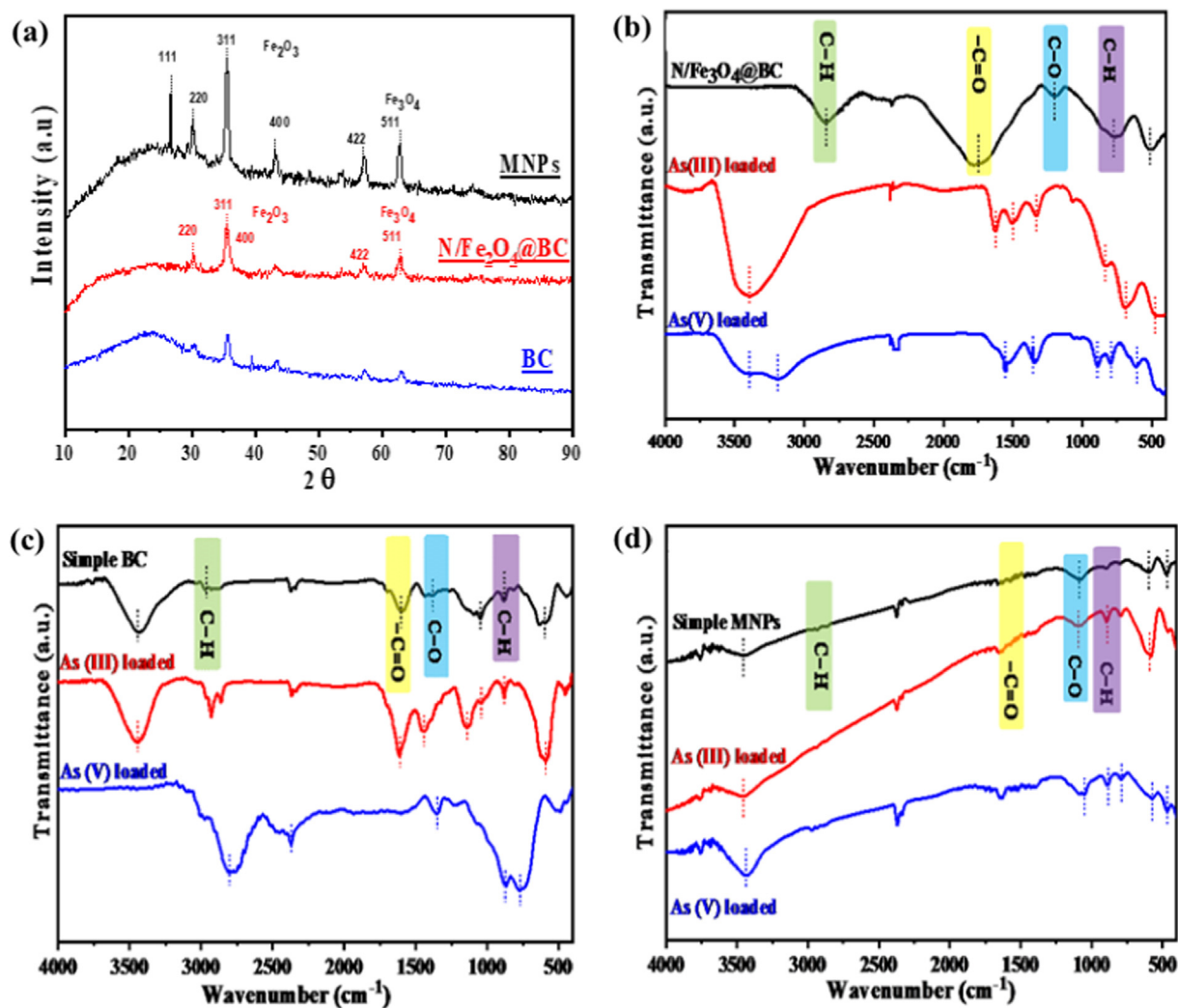
Fig 1. (a) XRD diffractogram and, (b–d) FTIR spectrum of all tested magnetite (N/Fe$_3$O$_4$@BC, BC, MNPs) before and after arsenic As (II) and As(V) adsorption.

O$_4$@BC)followed by 23.94 mg/g for As(III) and 12.45 mg/g for (As(V) in BC and 18.10 mg/g for As(III) and 16.30 mg/g for As(V) in MNPs. On the other hand, declining in % removal could be a better elaboration of higher ionic gradient built up against fixed low adsorbent dosage (fixed number of active surface sites) (Bellacosa et al., 1998). The increase in adsorption capacity by increasing adsorbate concentration could be better elaborated via **Eq. (2)**. The plausible explanation could be that the N/Fe$_3$O$_4$@BC might have more surface interaction sites after N doping and magnetic core shell structure depending upon adsorbate species interaction and the adsorbent interstitial space, those are responsible for adsorption process (Yu et al., n.d.).

3.2.2. Effect of contact time

Contact time is considered as an important parameter in adsorption studies for target pollutant elimination (Ajmal et al., 2018). The present study reports As(III & V) adsorption as a function of reaction time by determining the relationship between adsorption capacity and material surface characteristics. It was found that initial rapid As uptake rate was more obvious within a shorter period of time of 15, 30 and 60 min

for (N/Fe$_3$O$_4$@BC), BC and MNPs respectively. Thereafter, a declining pattern was started, where adsorption became slower until attained equilibrium (Fig. 3c & d). It can be seen that the surface adsorption was quick towards all tested materials surface sites in the order of (N/Fe$_3$O$_4$@BC) > BC > MNPs), respectively. All these characteristics clearly indicate the availability of more surface-active sites by producing external adsorption phenomenon towards nano-porous surface sites of tested adsorbents at the early stages of reaction, while in case of equilibrium point, porous and highly active surface adsorption site comparatively required more time to reach at equilibrium. This trend could be attributed to higher surface area and well porosity characteristics of the developed adsorbents, which should be further explored for potential realistic implication of tested materials. Conversely, a rapid uptake rate could be better explained in terms of larger driving forces existence at initial phases and therefore, initial rapid and highest adsorption capacity was more obvious (vertical curve established) for all tested material onto their porous surface sites (Nassar, 2010). The observed highest uptake capacity for As(III) and As(V) were (18.14, 9.87 mg/g) for (N/Fe$_3$O$_4$@-BC), (9.89, 8.12) for BC and (7.38, 8.56 mg/g) for MNPs.
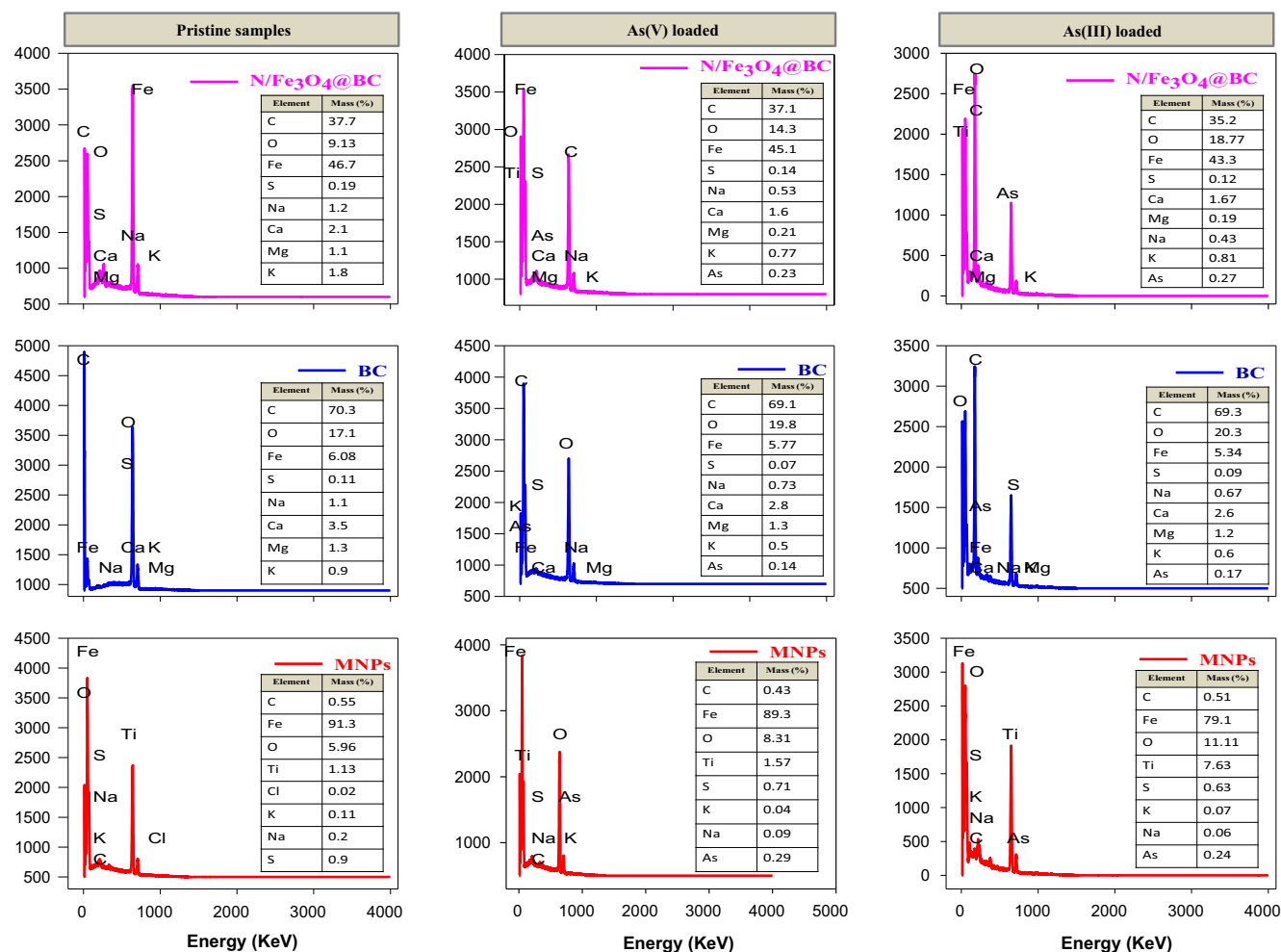
Fig. 2 EDS spectra of all tested adsorbent before and after As(III & V) adsorption.

3.2.3. Effect of reaction temperature

The adsorption of arsenic species as a function of temperature was evaluated within a temperature range from 288 to 328 K. The results Fig. 3e & f, demonstrated that adsorption capacity and % adsorption was enhanced with increasing temperature ranges from 288.15 K to 318.15 K, by a maximum adsorption capacity of 17.34 & 9.37 mg/g, for As(III) and (8.49 & 9.04) for As(V) onto (N/Fe$_3$O$_4$@BC), and MNPs, while for BC, the maximum adsorption of As(III) and As(V) was 10.16 $\pm$ 0.35 mg/g and 7.0 $\pm$ 0.14 mg/g) at 318.18 K and 328.15 K. The findings suggest that As removal is an endothermic process, and thereby temperature above ambient would be relatively suitable approach for higher adsorption for all tested adsorbents. The enhance in sorption capacity with increasing temperature could be due to decrease in solution viscosity and high free energy, which in turn promotes As diffusivity from external laminar layer to adsorbent pores (Nassar, 2010). However, a slightly decreasing pattern for adsorption capacity, and % removal was observed at 318 K for (N/Fe$_3$O$_4$@BC)and MNPs, and at 338 K for BC. It further suggests, that exothermic process was started thereafter. Therefore, it was implied that endothermic interactions mainly govern the As adsorption process between 318.15 and 328.15 K and afterward exothermic interactions might be possible at higher temperature (338.15 K) leading decreased sorption.

3.2.4. Effect of solution pH

The solution pH is considered as a main influential parameter during the adsorption process (Ajmal et al., 2020). The adsorption of As(V) and As(III) by all three tested adsorbents was examined over a wide range of pH from 3 to 11 as shown in Fig. 3g & h. The maximum As(V) adsorption of 11.31 mg/g for (N/Fe$_3$O$_4$@BC), 7.64 mg/g for BC and 9.56 mg/g for MNPs was observed at pH 6, pH 5 and pH 7 respectively, while pH 9, pH 7 and pH 8 were found to be the optimum pH values for As(III) adsorption at a rate of 16.10 mg/g, 9.04 mg/g and 8.05 mg/g for N/Fe$_3$O$_4$@BC, BC and MNPs respectively. It was found that alkaline conditions are unsuitable for both As(V) and As(III) adsorption onto MNPs, BC and (N/Fe$_3$O$_4$@BC). For example, the results of BC revealed that As adsorption increased, when pH increased from 3 to 5 for As (V) and 3 to 7 for As(III) and then declined on elevated pH, which indicated that As(III & V) adsorption onto BC surface sites was might be attributed to the Van der Waals inter-
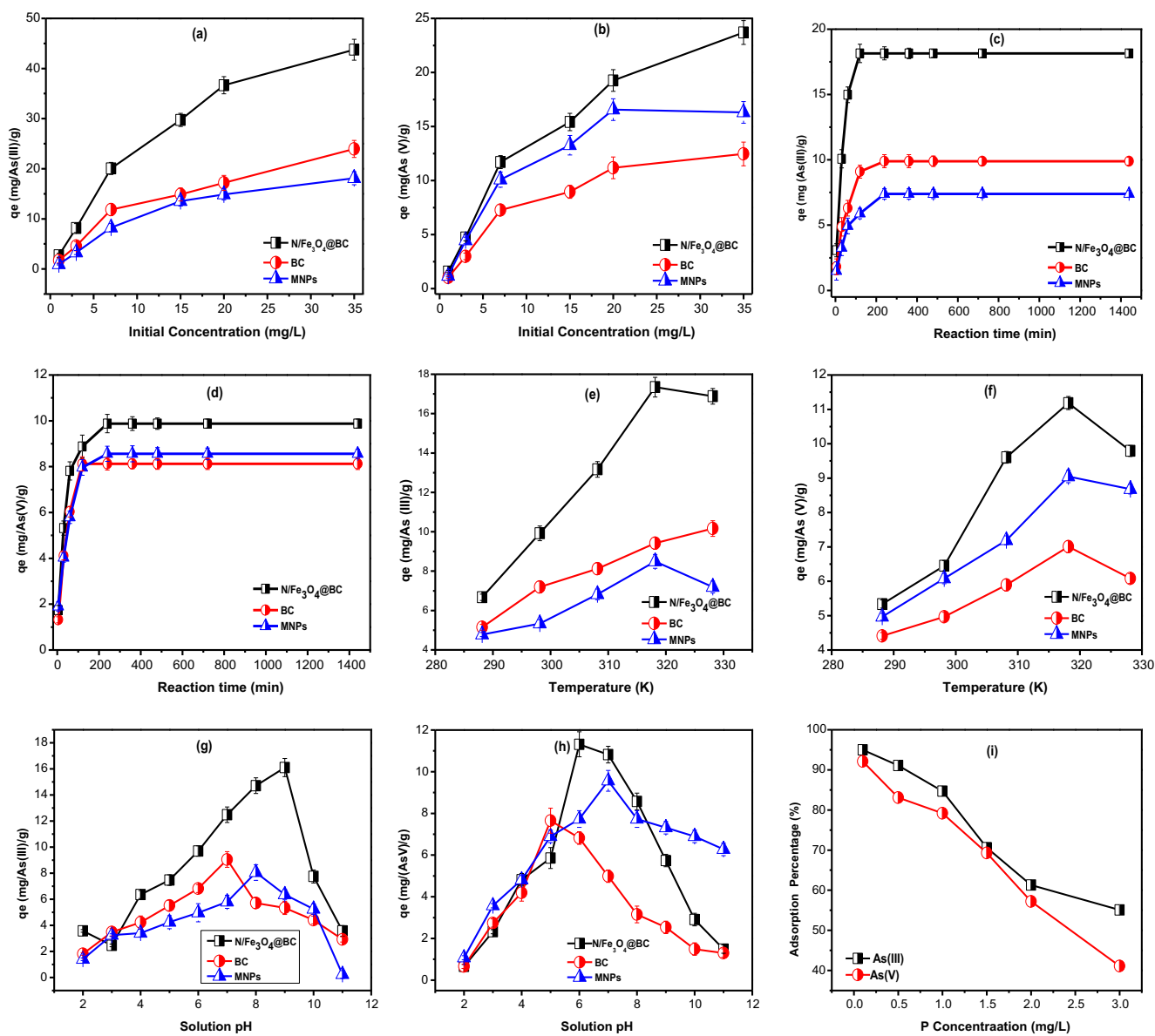
Fig. 3 Adsoprtion of Arsenic As (III & V) as a function of (a, b) initial concentration (c, d) reaction time (e, f) Temperature (g, h) Solution pH (i) Phosphate concentration.

action between BC surface and neutral H_3AsO_3 and H_2AsO_4 species. It is reported that dominant As(V) species are present as $H_2AsO_4^-$, $HAsO_4^{2-}$ and AsO_4^{3-} within the pH range between 2 and 14 respectively (Wei et al., 2016). Therefore, ability of tested adsorbent to adsorb metal ions decreases significantly by increasing pH. As we know that, lower pH is responsible for adsorbent surfaces sites protonation thus, higher adsorption is closely associated with higher electrostatic attraction as a result of increased protonation of material surface sites, which in turn enhanced aqueous arsenate anions, thereby boosting As(V) adsorption. With the rise of initial solution pH, the positively charged tested adsorbent surface sites gradually decreases, thus resulted an increase in electrostatic repulsion between liquid and solid interface hence, decreasing

adsorption. Similar finding has been reported for As(V) adsorption onto iron oxides and iron-containing oxides and biochar surfaces (Min et al., 2006).

On the other hand, As(III) species such as $H_3AsO_3^-$ and $H_2AsO_3^-$ are mainly found at pH lower than 9.2, while that of AsO_2 exists at pH higher than 9.2 (Zhang et al., 2016). Adsorption primarily occurred through the electrostatic attractions between negative As species and positively charged tested adsorbent surface sites. It means that the solution pH not only have significant impact onto material surface charge but also greatly influenced the speciation of As species in solution. More obviously, the MNPs could also play an important role to oxidize As(III) into As(V) based on solution pH. Therefore, higher adsorption of As(III) under near neutral pH (8)

conditions could be due to higher As(III) oxidation into As(V), mainly, because of dissolved oxygen as well as oxidizing intermediate at neutral pH than that of higher or lower pH condition (Zhang et al., 2016; Luo et al., 2012). Moreover, the decrease of adsorption efficiency for all tested adsorbent at alkaline pH is attributed to the more electrostatic repulsion between and negatively charged tested magnetite surface sites and anionic As species (AsO_2, $HAsO_4^{2-}$) (Luo et al., 2012). Because surplus OH^- groups exist at that stage and adsorption primarily might occurred via hydrogen bonding between adsorbate and adsorbent surface sites. Another possible reason could be higher competition between anionic (AsO_2, $HAsO_4^{2-}$) species and hydroxyl groups (OH^-) at higher pH condition (Shakoor et al., 2016). All tested adsorbents shown their point of zero charge about 8.2, 7.7 and 7.1. However, they can give rise to attraction below than these values or repulsion above these values depending upon adsorbate species charge and the adsorbent surface characteristics.

However, these results clearly indicate that the arsenic adsorption towards tested material surface sites was mainly controlled via two important phenomena: (i) electrostatic interaction (ii) As(III) oxidation between bulk liquid to solid interface (Shakoor et al., 2016). As(III) oxidation mainly occurred via contact with O_2 and the oxic conditions that leads to Fe(III) drying. As, anoxic conditions mostly responsible for magnetite transformation into maghemite that could also drives the oxidation process (Navarathna et al., 2019). Overall, the higher (Q_{max}) of (N/Fe$_3$O$_4$@BC)compared to pristine MNPs and BC indicates As (III &V) adsorption (N/Fe$_3$O$_4$@-BC)was due to surface complexation pathway (Luo et al., 2017).

3.2.5. Effect of phosphate on as adsorption

The result regarding the effect of phosphate onto As adsorption is displayed in Fig. 3i. In practical, ionic competition especially in real wastewater is more common due to multiple contaminant diversifications. It can be seen that as the concentration of phosphate was increased, then a significant reduction of both As(III) and As(V) was observed in (N/Fe$_3$O$_4$@BC)and MNPs samples. It means that the competing ions especially the phosphate have their significant impact over As species in real wastewater. It could be better explained in terms of similar charge properties as well as structural characteristics of phosphorus (P) in the form of PO_4^{3-}, which could be strongly bounded over positively charged (N/Fe$_3$O$_4$@BC)and MNPs surface sites than that by As species mainly depending upon solution pH and redox potential (Vatutsina et al., 2007). The previous results also corroborate our investigation, where the presence of P showed a strong binding interaction with MNPs. Tuutijarvi et al. (2012) also reported that P ions have enough capability to influence the adsorption of As(V) over iron based maghemite particles surface sites at pH 7 with an initial concentration > 3 mg/L (Tuutijärvi et al., 2012). In case of pristine BC, the P as competing ions didn't significantly affect As adsorption. It's because of negative BC surface sites, which in turn created an electrostatic repulsion phenomenon. Furthermore, the higher concentration ranges of both competing ions should also be investigated for their potential practical application.

3.3. Adsorption data modeling

3.3.1. Adsorption isotherm

In general, adsorption isotherm studies are critical to determine dominant adsorption phase existence between bulk liquid to solid interface for engineered adsorption systems designing (Safa and Bhatti, 2011). Thus, equilibrium adsorption data was evaluated by using two commonly employed Langmuir (Langmuir, 1918) and Freundlich models (Freundlich, 1906). The mathematical expressions are given below, while the graphical representation is presented in Fig. 4a & b.

$$q_e = \frac{KQC_e}{1 + KC_e} \quad \text{(Langmuir model)} \quad (4)$$

$$q_e = K_f C_e^{\ n} \quad \text{(Freundlich model)} \quad (5)$$

where, K indicates Langmuir bonding term related to bonding energies (L/mg), K_f is Freundlich affinity coefficient (L^n/mg^{n-1}g) C_e (mg/L) stands for residual concentration, Q (mg/g) denotes optimum Langmuir adsorption capacity, β (L/mg) represent equilibrium constant, K defines the adsorbed metal ions, and n specify the adsorption intensity. The n indicates Freundlich constant. The isotherm parameters for both As (III) and As(V) are listed in Table 2. The good fit of Langmuir model with higher correlation coefficient value (R^2) indicates the homogeneous phase of adsorbent surface sites. Moreover, its better description could be possible by calculating its separation factor value (dimensionless). Its mathematical form is given below.

$$R = (1/1 + bCo) \quad (6)$$

It represents the adsorption process is favorable, when $0 < R_L < 1$, unfavorable $R_L > 1$, linear adsorption $R_L = 1$ and $R_L = 0$, irreversible adsorption (Ngah et al., 2002). In the present study, the separation factor values were $0 < R_L < 1$, which further indicated that As adsorption as more favorable process through monolayer surface adsorption sites with optimum monolayer adsorption capacity of 66.80 mg g^{-1}, 34.28 mg g^{-1} and 28.25 mg g^{-1} for As(III) and 34.54 mg g^{-1}, 16.56 mg g^{-1} and 23.41 mg g^{-1} for As(V) in the order (N/Fe$_3$O$_4$@BC) > BC > MNPs, respectively. Conversely, the successful applicability of Freundlich model ($R^2 > 0.95$), indicated the favourability of As adsorption onto multilayer surface adsorption sites of tested adsorbents. Multilayer adsorption phase further indicated that adsorption was more suitable onto adsorbent for maximum pollutant removal in aqueous environments. On the other hand, the higher K_f values indicates easy removal of As(III) and As(V) ions from contaminated water to adsorbent surface sites. The Freundlich R^2 values for both As(III) and As(V) are presented in Table 2. In addition, adsorption intensity (1/n) is considered as important factor in adsorption process, which represents the adsorption from bulk liquid to solid interface. If the values of adsorption intensity n are < 1, then the adsorption is considered poor, while that in between 1 and 2 indicates the moderately difficult adsorption, on the other hand, if n lies in between 2 and 10, the adsorption is considered excellent. Even though, all the Freundlich R^2 values were > 0.95 indicating physical adsorption up to some extent, the values of 1/n, clearly indicate that high intensity of sorption towards all tested adsorbents (Tofan
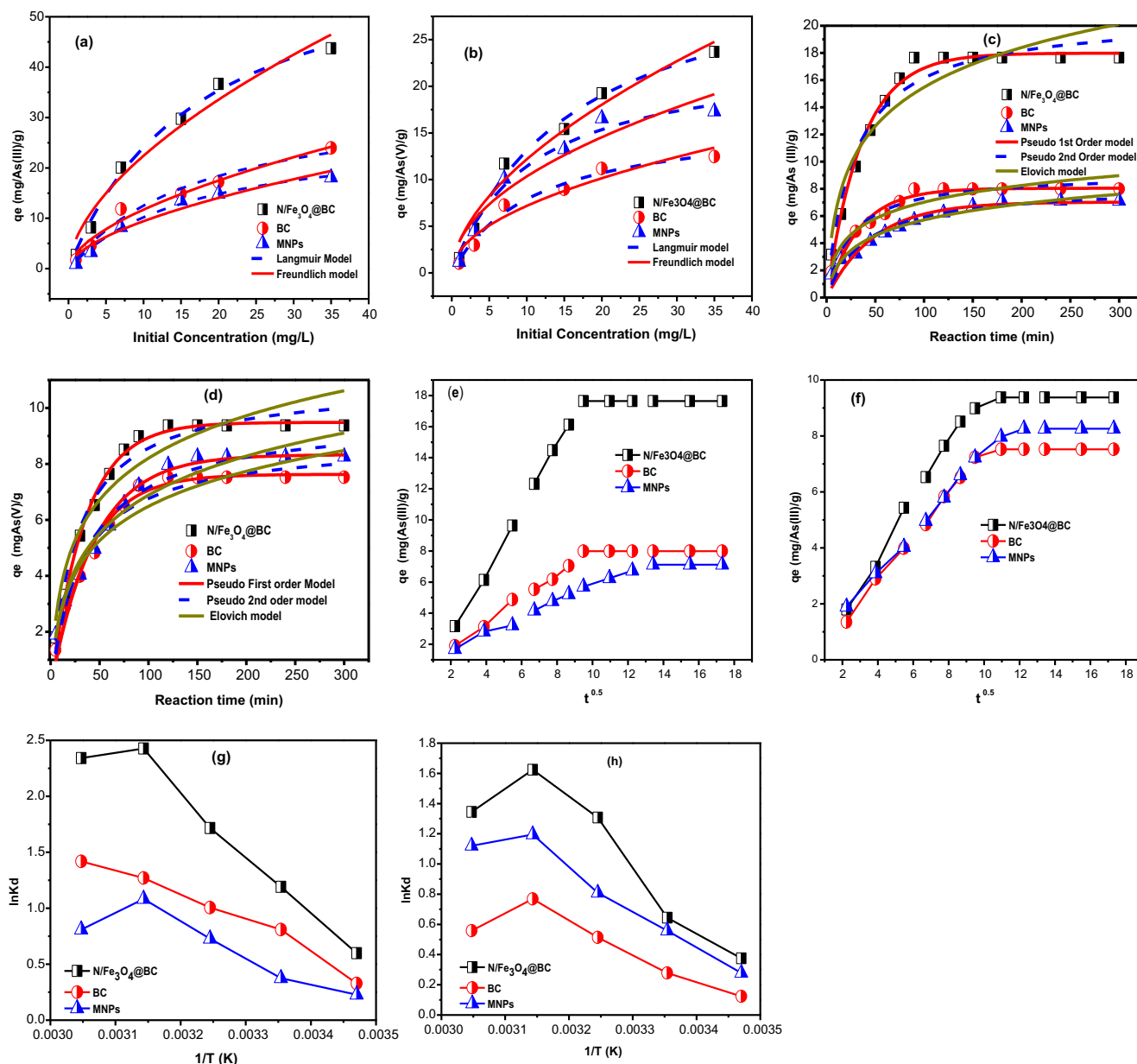
Fig. 4 The equilibrium and kinetic adsorption data modeling **(a, b)** As(III & V) data mdeling via Langmuir and Freundlich model **(c,d)** As(III & V) data interpretation via Pseudo 1st, 2nd and Elovich model **(e, f)** As(III & V) data interpretation via Intraparticle model.

Table 2 The profiles parameters and calculated Langmuir and Freundlich modeled values for As(III) and As(V) adsorption from aqueous solution by using $N/Fe_3O_4@BC$, BC and MNPs.

Material	Langmuir			Freundlich		
	Q (mg.g^{-1})	K(L/mg)	R_L^2	K_F (L^n/(mg$^{(n-1)}$·g)	n	R_F^2
As(III)- $N/Fe_3O_4@BC$	66.80	0.056	0.993	5.86	1.73	0.966
As(III)- BC	34.78	0.055	0.971	3.08	1.75	0.940
As(III)- MNPs	28.25	0.059	0.990	2.49	1.72	0.946
As(V)- $N/Fe_3O_4@BC$	34.54	0.061	0.987	3.30	1.78	0.962
As(V)- BC	16.56	0.091	0.978	2.27	2.04	0.905
As(V)- MNPs	23.41	0.095	0.976	3.32	1.96	0.942

et al., 2016). The calculated 1/n values are listed in Table 2, and were found higher than 1, indicating more than one mechanism involved in As adsorption towards all tested-adsorbents.

3.3.2. Adsorption kinetics

Adsorption kinetic data was evaluated by using Pseudo first order, pseudo second order, Elovich (Gerente et al., 2007) and intraparticle models (Choy et al., 2004). Mathematical expressions are given below, while the graphical representation is presented in Fig. 4c & d.

$$\frac{dq_t}{q_t} = K_1(q_e - q_t)^2 \text{ (Pseudo first order model)} \tag{7}$$

$$\frac{dq_t}{q_t} = K_2(q_e - q_t)^2 \text{ (Pseudo second order model)} \tag{8}$$

$$\frac{dq_t}{q_t} = \alpha exp(-\beta qt) \text{ (Elovich model)} \tag{9}$$

$$q_t = K_d \, t^{1/2} + C \text{ (Intraparticle model)} \tag{10}$$

where; q_e, and q_t (mg/g) are the equilibrium metal ions adsorption capacity at time t, k_1 and k_2 are first and second order apparent rate constants, while that of α indicates initial adsorption coefficient mg/g/h) and β indicates desorption constant (g/mg). The experimental q (mg/g) and calculated q_e, (mg/g) values for maximum adsorption of As(III) and As(V) were compared. When experimental and calculated values of specific models are closer the reference, model would be considered to fit the experimental data very well. Another parameter is the correlation coefficient (R^2), if its value is ≥ 0.95, then the model would be considered most suitable for kinetic experimental data interpretation. Conversely, the intraparticle and Elovich model were interpreted based on β, K_d and R^2 values. In case of intraparticle, the model was considered to be fit if Q_t vs $t^{1/2}$ plot is linear. All the calculated modeled values (q_1, q_2, β, C) and rate constant (k_1, k_2, α and K_d) are listed in Table 3.

The fitted curves for all models are presented in Fig. 4c & d. Firstly, the assumption was made for intraparticle model Fig. 3e & f, where R^2 values were ≤ 0.95 and straight lines were not passing through the origin and bilinear trend was more obvious (C $\neq$ 0), then the intraparticle diffusion as rate limiting step was rejected for all the tested adsorbents and the initial linear trend always indicates the involvement of film diffusion. Hence, the larger values of intercept clearly indicate the involvement of mutually external forces via (film and intra-

particle), which are in counter play for As(III, V) adsorption onto tested adsorbent surfaces sites, and intraparticle is not rate limiting step (Tofan et al., 2016). Secondly, it was noted that higher correlation coefficient values of pseudo first order (0.99–0.98) rather than that of pseudo second (0.95–0.90) and Elovich (0.88–0.79) indicate the successful suitability for both As(III) and As(V), and the calculated (qe_{cal}) and the experimental values (qe_{cal}) were also found to be closer with each other. Thus, higher pseudo first order model correlation coefficient values than pseudo second order, thus implying the physio-sorption mechanism as more effective. Thus, our results totally contradict with certain previous investigation where As(III &V) adsorption over magnetite nano-particles, biochar and magnetic biochar were primarily governed by chemisorption mechanism owing to best fitting of experimental data to pseudo second order model (Jiaming et al., 2018). On the other hand, the sorption rate constant values of N/Fe$_3$O$_4$@/BC particles is higher than BC particles, thus these findings further suggest that As(III, V) sorption is not solely depends upon material superior surface characteristics, because if it is the cause then BC and MNPs must have larger adsorption rate constant. It further indicates that sorption via surface functional group might be more dominant over (N/Fe$_3$O$_4$@BC) particle than that of other tested adsorbents. In reality, by seeing BET surface area characteristics, one would expect MNPs and BC to be evidence for superior adsorption rather than (N/Fe$_3$O$_4$@BC) in aqueous solution.

3.3.3. Adsorption thermodynamics

Adsorption thermodynamics is an important parameter in adsorption studies. Variations in temperature plays an important role to evaluate material adsorption performance. The adsorption of As(III) and As(V) to materials surface sites was performed by varying the temperature from 288.15 K to 328.15 K. Vent Hoff equation was used for data fitting as manifested in Fig. 4e & f.

$$K_d = \frac{C_o - C_e}{C_e} \tag{11}$$

The C_e and C_o (mg/L) stands for final and initial metal ions concentrations. The Gibb's free energy change ($\Delta G°$), was calculated through K_d by Eq. (11) and Eq. (12).

$$\Delta G° = -RTlnK_c \tag{12}$$

$$\ln K_d = -\frac{\Delta G°}{RT} = -\frac{\Delta H°}{RT} + \frac{\Delta S°}{R} \tag{13}$$

Table 3 The profile parameter and calculated modeled values for As(III) and As(V) adsorption onto Fe$_3$O$_4$@N/BC, BC and MNPs.

Material	Q_{exp}	Pseudo 1st order			Pseudo 2nd order			Elovich			Intraparticle		
		qe (mg/g)	K_1 (1/h)	R^2	qe (mg/g)	K_1 (g/mg/h)	R^2	α (mg/g)	β (g/mg)	R^2	K_d (mg/g/min^{-1})	C (mg/g)	R^2
N/Fe$_3$O$_4$@BC	17.6	17.9	0.029	0.988	20.7	0.0017	0.951	1.52	0.23	0.897	0.20	1.1	0.739
BC	7.99	8.04	0.027	0.968	9.14	0.0043	0.943	0.87	0.55	0.914	0.39	2.5	0.765
MNPs	7.12	7.29	0.026	0.955	8.22	0.0031	0.941	0.56	0.43	0.941	0.66	2.6	0.907
As (V)													
N/Fe$_3$O$_4$@BC	9.37	9.48	0.028	0.992	10.89	0.0037	0.953	0.86	0.55	0.909	0.37	2.0	0.93
BC	7.52	7.62	0.025	0.982	8.81	0.0033	0.958	0.60	0.54	0.920	1.93	2.2	0.94
MNPs	8.26	8.33	0.022	0.962	9.71	0.0028	0.946	0.55	0.49	0.948	0.50	2.4	0.89

Table 4 Adsorption of As(III) and As(V) as a function of temperature. Thermodynamics adsorption data interpratation through ven't hoff equation.

Temperature (K)	K_d	$-\Delta G^\circ$ (J/mol)	ΔH° (kj·mol^{-1})	ΔS° (j·mol K^{-1})	R^2
N/Fe₃O₄@BC As(III)					
288.15	1.82	1434.1	37.4	135.3	0.9412
298.15	3.29	2950.8			
308.15	5.56	4397.0			
318.15	11.3	6419.9			
328.15	10.4	6387.1			
BC					
288.15	1.38	784.6	20.9	76.1	0.968
298.15	2.24	2006.2			
308.15	2.73	2577.1			
318.15	3.56	3359.7			
328.15	4.13	3870.8			
MNPs					
288.15	1.26	546.2	14.9	53.8	0.760
298.15	1.46	930.8			
308.15	2.07	1864.5			
318.15	2.95	2862.9			
328.15	1.75	2208.0			
N/Fe₃O₄@BC As(V)					
288.15	1.46	899.5	23.3	84.5	0.796
298.15	1.90	1596.4			
308.15	3.70	3349.4			
318.15	5.07	4295.8			
328.15	3.84	3668.2			
BC					
288.15	1.13	294.8	10.9	39.0	0.752
298.15	1.32	690.1			
308.15	1.67	1315.4			
318.15	2.16	2033.5			
328.15	1.39	1521.6			
MNPs					
288.15	1.32	666.9	18.4	66.3	0.927
298.15	1.75	1382.5			
308.15	2.25	2073.4			
318.15	3.31	3162.1			
328.15	3.07	3056.3			

The R is the ideal gas constant with value 8.314 J·mol^{-1}·K^{-1} and T is the temperature (K). Thus, a graph between lnKd v/s 1/T gives the values of enthalpy (ΔH) and entropy (ΔS) change through its slope and intercepts values. All the calculated modeled parameters i.e., ΔH°, ΔG°, ΔS° and K_d with R^2 for all temperatures to all tested adsorbents are listed in Table 4. From the concern **Table**, it can be seen that K_d values were enhancing by increasing temperature from (288.15 – 328.15 K). Thus, increasing Kc and positive ΔH° values suggest that adsorption is endothermic in nature. On the other hand, negative Gibb's free energy ΔG° values suggest adsorption is mainly physical, spontaneous and more favorable by increasing temperature from 288.15 K to 328.15 K. The entropy changes values (ΔS° values for all tested adsorbents were in positives range). These positive entropies change values, further indicates the higher randomness with quick interaction between adsorbate/adsorbent interfaces by increasing thermostat temperature. The increase of sorption with temperature could be due to rapid reaction between As(III) and As(V)

ions and adsorbent surface functional groups at higher temperature due to decreasing solution viscosity and high free energy, which in turn promotes the As diffusivity from external laminar layer to adsorbent fine pores (Xiong et al., 2015). Furthermore, it has been shown in literature, that at $\Delta H^\circ < 25$ kJ mol^{-1}, the acting forces during adsorbate/adsorbent interaction would be Van der Waals forces and might be ascribed to physisorption but if ΔH° values are in between 40 kJ mol^{-1} and 200 kJ mol^{-1}, then the main dominant forces would be the chemical bonding, thereby indicating the chemical adsorption phenomena (Xiong et al., 2015).

3.4. Potential adsorption mechanism

Proposed adsorption mechanism was investigated using a series of parameters and FTIR spectra. The FTIR spectra of all tested adsorbents (N/Fe₃O₄@BC, BC and MNPs) before and after As adsorption are provided in Fig. 1**b–d**. As it can be seen from the virgin spectra of BC and MNPs, that all tested materials were found to have almost five distinct bands at 581, 579, 563 and 937, 937 and 933, 1143, 1141 and 1129, 1635, 1631 and 1634, 3440, 3431 and 3435 cm^{-1} frequencies. These bands indicate Fe-OH stretching and bending vibrations hydroxyl groups, which are converted from the iron oxide in transient complex species form such as Fe-OH,-Fe(OH)₂, or FeO(OH) onto tested (N/Fe₃O₄@BC), BC and MNPs surface sites (Tang et al., 2011). The band that shifts from 711 to 790 and 810–899 cm^{-1} as well as 937, 937 and 933 cm^{-1} in to 909, 904 and 915 cm^{-1} and 901, 922 and 917 cm^{-1}, indicates As adsorption is might be due to As-O stretching band vibration in a partial As$^{3+} \rightarrow$ Fe substitution (Baig et al., 2014). In addition, peaks attributable to C—H alkene (801–899 cm^{-1}), C—O aloxy (1221–1238 cm^{-1}), –C=O stretch (1508–1539 cm^{-1}), C—H stretch (2876–2980 cm^{-1}) were also observed for (N/Fe₃O₄@BC), BC and MNPs. After As(III) adsorption these band were shifted to 895, 899 and 889 cm^{-1}, for (N/Fe₃O₄@BC), BC and MNPs. Similarly, the shift in band with corresponding peaks 1219.4, 1222.2 and 1242.3 was also observed after As(V) adsorption over, BC and MNPs (Alam et al., 2018). Moreover, after As(III) adsorption some peaks (583, 585 and 587) were shifted to 576, 580 and 579 for (N/Fe₃O₄@BC), BC and MNPs. In addition, some new peaks appeared at 683, 677, 763, 644 and 681 cm^{-1}, which indicate some inorganic As compound adsorption. Intensities of some corresponding peaks at 1635, 1631, 1634 cm^{-1} and $\sim$3440, 3431, 3435 cm^{-1} were seems to be decreased, which clearly indicates surface OH groups involvement, which might be replaced by As(III) and As(V) after adsorption to form Fe-O As(III)/As(V) complex. However, broad band at 3440, 3450, 3460 cm^{-1} corresponding to OH stretching model shows hydrogen bonding and physisorbed water molecules (Chen et al., 2011). The peak originally at 3440 cm^{-1} which is commonly associated with As(III) and As(V) was shifted to 3387 cm^{-1} and 3464 cm^{-1} suggesting involvement of N—H amino (stretch) group. At the same time, the peak at 1587 cm^{-1} was shifted to 1595 cm^{-1} indicating involvement of N—H amino (bending) group. This is a clear indication of the successful adsorption of As(III) and As(V) over (N/Fe₃O₄@BC), BC and MNPs nanoparticles via interaction with OH$^-$ groups. Moreover, higher adsorption of As(V) than that As(III) on MNPs, could be clearly seen as the absorption peak in the range of 810–899 cm^{-1} is more intense

than that of 711–790–792 cm^{-1} over MNPs surface sites (Zhu et al., 2009). Overall FTIR spectra from 2800 to 3400 cm^{-1} and 650–1750 cm^{-1} indicate As species binding with adsorbent. Hence, all FTIR peaks variation after arsenic As adsorption indicated the involvement of surface, Fe-O, carbonyl group and specifically hydroxyl groups (Shakoor et al., 2016). The results of pH analysis as earlier discussed are consistent, where hydroxyl plays an important role with FTIR assumption during adsorption process.

However, the pH results clearly indicate that the As adsorption towards tested adsorbents surface sites was mainly controlled via two important phenomenon: (i) electrostatic interaction and (ii) Oxidation of As(III) into As(V) between bulk liquid to solid interface (Shakoor et al., 2016). Moreover, another interesting phenomenon was noticed whenever initial metal concentration was increased, then the final pH was found to be decreased. This indicates that the adsorption is dominated by an ion-exchange mechanism by BC and (N/Fe$_3$O$_4$@BC)surface sites substantial oxygen content including hydroxyl and carboxyl groups, and could be considered as active center for ion exchange phenomenon (Klimmek et al., 2001). Data better fitted to Langmuir model clearly indicates the dominance of monolayer adsorption via surface complex pathway, as the affinity of As to Fe/BC, and As–Fe complexation on (N/Fe$_3$O$_4$@BC) after H$^+$ ions exchange in aqueous solution. Thus, our finding clearly demonstrates adsorption via electrostatic attraction, ion exchange and surface complexation pathways. Therefore, ion exchange mechanism could not be ignored during whole adsorption process. All in all, the deeper insights and multiple potential adsorption pathways further required a wide range of high level various spectroscopic techniques analysis.

3.5. Desorption characteristics

Recycling process of tested material after As ions removal is an important parameter for reducing the pollutant load in the environment (Naciri et al., 2019). Many studies have evaluated the desorption and spent adsorbents regeneration to determine their potential continuous application in pollutant removal. Desorption of As loaded adsorbent was determined by using distilled water, NaOH and H$_2$SO$_4$ solutions (Fig. 5a & b). Distilled water resulted into low desorption, which was found to be nearly 26.3, 23.6 and 24.1 % for As(III) in the order of,
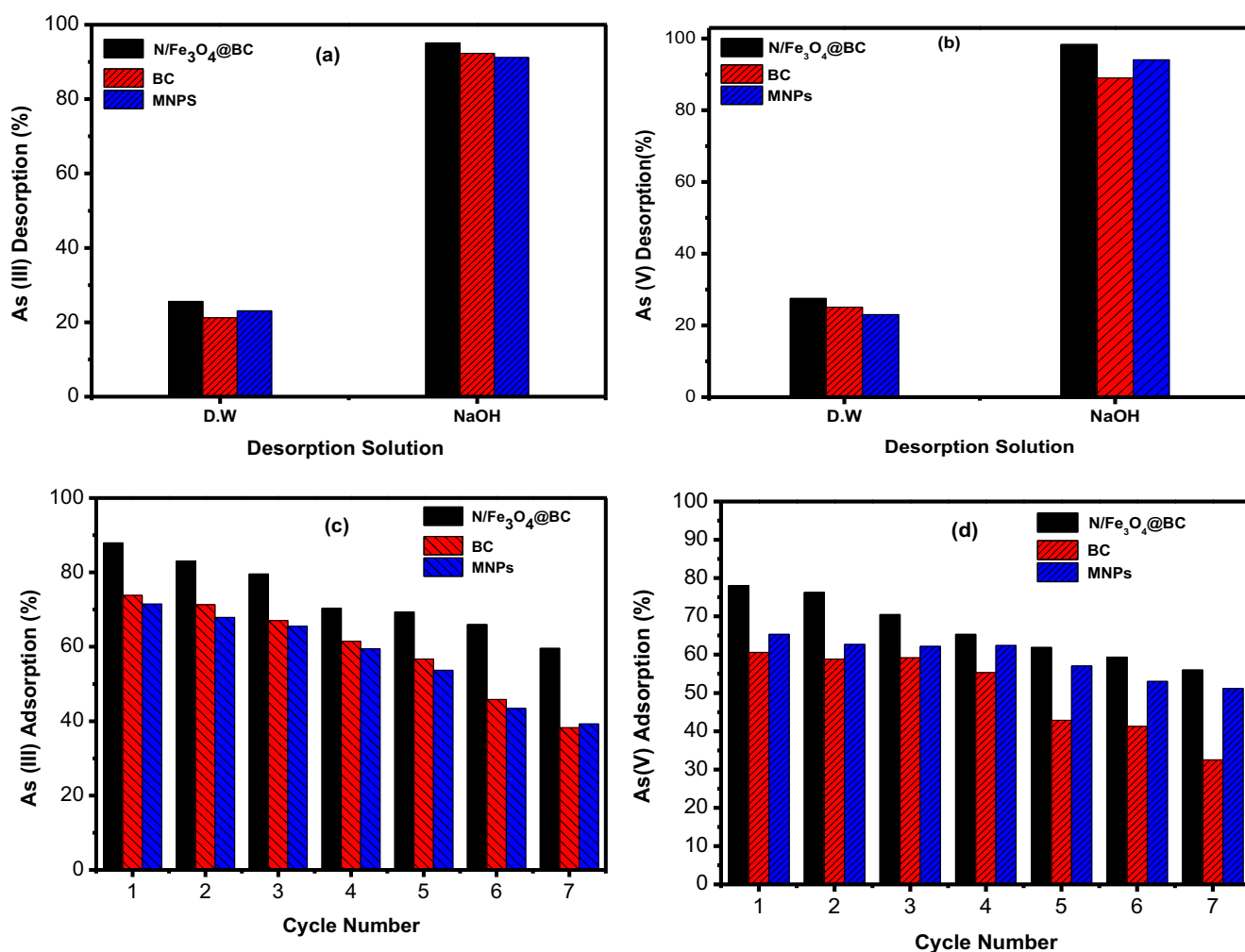
Fig. 5 Desorption performance of all tested adsorbents for As(III) and As(V) **(a,b)** as well as subsequesnt adsorption/desorption cycles **(c, d)** by using distilled water, alkaline eluents.

BC > MNPs > (N/Fe₃O₄@BC). The As(V) desorption was 27.5, 24.5 and 25.1 % in distilled water in the order of (N/Fe₃O₄@BC), BC and MNPs Fig. 5**a & b**. Maximum As(III) desorption up to 87.1, 91.3 and 81.1 % was observed in alkaline environment from (N/Fe₃O₄@BC), BC and MNPs. On the other hand, As(V) desorption from (N/Fe₃O₄@BC), BC and MNPs was 96.3 %, 94.2 % and 95.1 %. Herein, also the low desorption of As(III) compared to As(V) was also observed and that might be As(III) oxidation into As(V), which clearly proved in pH investigation of As(III) into As(V). Even though, the low concentration of As(V) was also observed in As(III) desorption solution. But the surprising fact is the As(III) concentration was also observed in As(V) desorption solution in the order of MNPs > (N/Fe₃O₄@BC) > BC. So, the As(V) reduction phenomenon up to some extent could not be ignored during whole adsorption process. The obtained data indicates that spent adsorbents could be used up to 5th regeneration cycles without substantial loss of adsorption capacity during consecutive adsorption/desorption cycles. The (N/Fe₃O₄@BC) particle showed better desorption as well as higher adsorption performance after 5 regeneration cycles owing to its good magnetic properties and easy separation Fig. 5**c & d**. After consecutive adsorption desorption cycles the higher adsorption performance of (N/Fe₃O₄@BC) and MNPs particle might be due to the breakdown of large bulks into small one which resulted into exposure of new surface adsorption sites for maximum pollutant adsorption. On the other hand, a complete desorption was not achieved throughout the experimentation, which can be better explained in terms of adsorbent surface sites passivation, strong chemical binding between adsorbent and adsorbate as well as oxidation/reduction reaction during consecutive adsorption/ desorption cycles (H.J. A et al.,2015). Decrease in adsorption of all tested adsorbents with the passage of consecutive regeneration cycles is due to loss of adsorption surface sites. Similar results of decrease in adsorption have been reported in literature (Kizito et al., 2017). Therefore, these materials could be used as cost-effective alternative over other adsorbents with remarkable regeneration potential to remediate As contaminated water and side remediation system.

4. Conclusions

In this study, the application of nitrogen doped magnetic biochar (N/Fe₃O₄@BC) as potential adsorbent for As removal from aqueous solution was evaluated. The obtained results revealed that As adsorption was strongly affected by variation in material structural characteristics and solution pH. Higher adsorption performance by (N/Fe₃O₄@BC) was observed compared to pristine BC and MNPs. Overall, As(III) adsorption was found to be in the order of (N/Fe₃O₄@BC) > BC > MNPs, while in case of As(V) the MNPs exhibited higher adsorption than BC, and a reverse order was observed (N/Fe₃O₄@BC) > MNPs > BC. Kinetic and isotherm data were satisfactorily tailored by Pseudo first order and Langmuir model thereby suggesting the physio-chemical process was the rate-limiting step. The kinetic results further indicated that the external mass transfer and physisorption affect arsenic adsorption more significantly. An alkaline eluent was a better desorption strategy allowing material regeneration up to 5 adsorption cycles without significant loss in adsorption capacity. Based on the monolayer sorption maximum and the potential to regenerate/ recover sorption capacity the developed magnetically modified and *N*-doped biochar could prove an effective adsorbent for the treatment of low-to moderately As contaminated water.

Declaration of Competing Interest

The authors declare that they have no known competing financial interests or personal relationships that could have appeared to influence the work reported in this paper.

Appendix A. Supplementary material

Supplementary data to this article can be found online at https://doi.org/10.1016/j.arabjc.2022.104209.

References

Adeo, A.I., Ofudje, A.E., Mopelola, A.I., Sarafadeen, O.K., 2011. Equilibrium, kinetics and thermodynamic studies of the biosorption of Mn (II) ions from aqueous solution by raw and acid-treated corncob biomass. BioResources 6, 4117–4134.

Ahmed, S., Ashiq, M.N., Li, D., Tang, P., Feng, Y., 2018. Carbon fiber paper@MgO films: in situ fabrication and high-performance removal capacity for phosphate anions. Environ. Sci. Pollut. Res. 25, 34788–34792.

Ahmed, S., Rehman, H.U., Ali, Z., Qadeer, A., Haseeb, A., Ajmal, Z., 2021. Solvent assisted synthesis of hierarchical magnesium oxide flowers for adsorption of phosphate and methyl orange: kinetic, isotherm, thermodynamic and removal mechanism. Surf. Interf. 23, 100953.

Z. Ajmal, A. Muhmood, M. Usman, S. Kizito, J. Lu, R. Dong, S. Wu, Phosphate removal from aqueous solution using iron oxides: Adsorption, desorption and regeneration characteristics, Journal of Colloid & Interface Science, (2018) S0021979718306039

Ajmal, Z., Usman, M., Anastopoulos, I., Qadeer, A., Zhu, R., Wakeel, A., Dong, R., 2020. Use of nano-/micro-magnetite for abatement of cadmium and lead contamination. J. Environ. Manage. 264, 110477.

Ajmal, Z., Muhmood, A., Dong, R., Wu, S., 2020. Probing the efficiency of magnetically modified biomass-derived biochar for effective phosphate removal. J. Environ. Manage. 253, 109730.

Ajmal, Z., Naciri, Y., Hsini, A., Bresolin, B.M., Qadeer, A., Nauman, M., Arif, M., Irshad, M.K., Khan, K.A., Djellabi, R., 2021. C.L. Bianchi, M. Laabd, A. Albourine, R. Dong, Prospects of Photocatalysis in the Management of Nitrate Contamination in Potable Water. In: Oladoja, N.A., Unuabonah, E.I. (Eds.), Progress and Prospects in the Management of Oxyanion Polluted Aqua Systems. Springer International Publishing, Cham, pp. 185–217.

Alam, M.A., Shaikh, W.A., Alam, M.O., Bhattacharya, T., Chakraborty, S., Show, B., Saha, I., 2018. Adsorption of As (III) and As (V) from aqueous solution by modified Cassia fistula (golden shower) biochar. Appl. Water Sci. 8.

Ali, S., Rizwan, M., Shakoor, M.B., Jilani, A., Anjum, R., 2020. High sorption efficiency for As(III) and As(V) from aqueous solutions using novel almond shell biochar. Chemosphere 243.

Auta, M., Hameed, B.H., 2013. Acid modified local clay beads as effective low-cost adsorbent for dynamic adsorption of methylene blue. J. Ind. Eng. Chem. 19, 1153–1161.

Baig, S.A., Zhu, J., Muhammad, N., Sheng, T., Xu, X., 2014. Effect of synthesis methods on magnetic Kans grass biochar for enhanced As (III, V) adsorption from aqueous solutions. Biomass Bioenergy 71, 299–310.

Bakouri, H.E., Morillo, J., Usero, J., Vanderlinden, E., Vidal, H., 2010. Effectiveness of acid-treated agricultural stones used in biopurification systems to avoid pesticide contamination of water resources caused by direct losses: part I. equilibrium experiments and kinetics. Bioresour. Technol. 101, 5084–5091.

Baokang, D., Yipeng, C., Hanwei, W., Bo, C., Chunde, J., Qingfeng, S., 2018. Preparation of high mechanical performance nano-Fe$_3$-O$_4$/wood fiber binderless composite boards for electromagnetic absorption via a facile and green method. Nanomaterials 8, 52.

Bellacosa, A., Chan, T.O., Ahmed, N.N., Datta, K., Malstrom, S., Stokoe, D., Mccormick, F., Feng, J., Tsichlis, P., 1998. Akt activation by growth factors is a multiple-step process: the role of the PH domain. Cornell University Press 17, 313–325.

Brini, L., H'Maida, K., Imgharn, A., Hsini, A., Naciri, Y., Ajmal, Z., Bouziani, A., Boulahya, A., Arahou, M., Bakiz, B., Albourine, A., Fekhaoui, M., 2021. Synthesis and characterisation of PANI-coated Heliotrope Leaves (PANI@HL) with high clean-up capacity for Orange G dye from aqueous media. Int. J. Environ. Anal. Chem. 1–17.

Chakraborti, D., Rahman, M.M., Ahamed, S., Dutta, R.N., Pati, S., Mukherjee, S.C., 2016. Arsenic groundwater contamination and its health effects in Patna district (capital of Bihar) in the middle Ganga plain, India. Chemosphere 152, 520–529.

Chen, B., Chen, Z., Lv, S., 2011. A novel magnetic biochar efficiently sorbs organic pollutants and phosphate. Bioresour. Technol. 102, 716–723.

Chen, H., Gao, Y., El-Naggar, A., Niazi, N.K., Sun, C., Shaheen, S. M., Hou, D., Yang, X., Tang, Z., Liu, Z., 2022. Enhanced sorption of trivalent antimony by chitosan-loaded biochar in aqueous solutions: characterization, performance and mechanisms. J. Hazard. Mater. 425, 127971.

Chen, W., Mo, J., Du, X., Zhang, Z., Zhang, W., 2019. Biomimetic dynamic membrane for aquatic dye removal. Water Res. 151, 243–251.

Chen, S.P., Wang, J.H., Chen, H.W., Chen, Z.L., Hou, J., Xu, X.J., Chen, J.B., Liu, Z.J., 2011. 20 W all fiber supercontinuum generation from picosecond MOPA pumped photonic crystal fiber. Laser Phys. 21, 519–521.

Choy, K.K.H., Porter, J.F., McKay, G., 2004. Intraparticle diffusion in single and multicomponent acid dye adsorption from wastewater onto carbon. Chem. Eng. J. 103, 133–145.

Dhar, R.K., Zheng, Y., Rubenstone, J., van Geen, A., 2004. A rapid colorimetric method for measuring arsenic concentrations in groundwater. Anal. Chim. Acta 526, 203–209.

Duan, X., Liu, J., Hao, J., Wu, L., He, B., Qiu, Y., Zhang, J., He, Z., Xi, J., Wang, S., 2018. Magnetically recyclable nanocatalyst with synergetic catalytic effect and its application for 4-nitrophenol reduction and Suzuki coupling reactions. Chem. Eng. Sci. 130, 806–813.

Essekri, A., Aarab, N., Hsini, A., Ajmal, Z., Laabd, M., El Ouardi, M., Ait Addi, A., Lakhmiri, R., Albourine, A., 2022. Enhanced adsorptive removal of crystal violet dye from aqueous media using citric acid modified red-seaweed: experimental study combined with RSM process optimization. J. Dispersion Sci. Technol. 43, 1359–1372.

Ff, A., Qi, W.B., 2011. Removal of heavy metal ions from wastewaters: a review-ScienceDirect. J. Environ. Manage. 92, 407–418.

Fisher, M.B., Williams, A.R., Jalloh, M.F., Saquee, G., Bain, R., Bartram, J.K., 2015. Microbiological and chemical quality of packaged sachet water and household stored drinking water in freetown, Sierra Leone. PLoS ONE 10.

Freundlich, H.M.F., 1906. Over the adsorption in solution. J. Phys. Chem. 57, 385–471.

Gerente, C., Lee, V.K.C., Cloirec, P.L., McKay, G., 2007. Application of chitosan for the removal of metals from wastewaters by adsorption mechanisms and models review. Crit. Rev. Environ. Sci. Technol. 37, 41–127.

Gong, Y.L., Hua, Z., Ye, T.F., 2011. Heat flow density in bohai bay basin: data set compilation and interpretation. Procedia Earth Planet. Sci. 2, 212–216.

H.J. A, F.G. B, H.A.T. C, S.M.H.A. D, Study of the adsorption of Cd (II) from aqueous solution using zeolite-based geopolymer, synthesized from coal fly ash; kinetic, isotherm and thermodynamic studies, Arabian Journal of Chemistry, 8 (2015) 837-849.

Hao, O.J., Kim, H., Chiang, P.C., 2000. Decolorization of wastewater. Crit. Rev. Environ, Sci.

D. Harikishore Kumar Reddy, S.-M. Lee, Magnetic biochar composite: Facile synthesis, characterization, and application for heavy metal removal, Colloids and Surfaces A: Physicochemical and Engineering Aspects, 454 (2014) 96-103.

A. Hayat, M. Sohail, T.A. Taha, S. Kumar Baburao Mane, A.G. Al-Sehemi, A.A. Al-Ghamdi, W.I. Nawawi, A. Palamanit, M.A. Amin, A.M. Fallatah, Z. Ajmal, H. Ali, W. Ullah Khan, M. Wajid Shah, J. Khan, S. Wageh, Synergetic effect of bismuth vanadate over copolymerized carbon nitride composites for highly efficient photocatalytic H$_2$ and O$_2$ generation, J. Colloid. Interf. Sci., 627 (2022) 621-629.

A. Hayat, M. Sohail, W. Iqbal, T.A. Taha, A.M. Alenad, A.G. Al-Sehemi, S. Ullah, N.A. Alghamdi, A. Alhadhrami, Z. Ajmal, A. Palamanit, W.I. Nawawi, H.S. AlSalem, H. Ali, A. Zada, M.A. Amin, Molecular engineering optimized carbon nitride photocatalyst for CO$_2$ reduction to solar fuels, (2022) 100483.

Hayat, A., Sohail, M., Anwar, U., Taha, T.A., El-Nasser, K.S., Alenad, A.M., Al-Sehemi, A.G., Ahmad Alghamdi, N., Al-Hartomy, O.A., Amin, M.A., Alhadhrami, A., Palamanit, A., Mane, S.K.B., Nawawi, W.I., Ajmal, Z., 2022. Enhanced photocatalytic overall water splitting from an assembly of donor-π-acceptor conjugated polymeric carbon nitride. J. Colloid Interface Sci. 624, 411–422.

He, K., Lv, T., Wu, S., Guo, L., Ajmal, Z., Luo, H., Dong, R., 2016. Treatment of alkaline stripped effluent in aerated constructed wetlands: feasibility evaluation and performance enhancement. Water 8, 386.

Jiaming, F., Xin, X., Qunli, N., Qi, L., Jing, F., Qian, C., Xiaodong, S., Liping, L., 2018. Enhanced As (V) removal from aqueous solution by biochar prepared from iron-impregnated corn straw. J. Chem. 2018, 1–8.

Jin, H., Capareda, S., Chang, Z., Gao, J., Xu, Y., Zhang, J., 2014. Biochar pyrolytically produced from municipal solid wastes for aqueous As(V) removal: adsorption property and its improvement with KOH activation. Bioresour. Technol. 169, 622–629.

Khorram, M.S., Zheng, Y., Lin, D., Zhang, Q., Fang, H., Yu, Y., 2016. Dissipation of fomesafen in biochar-amended soil and its availability to corn (Zea mays L.) and earthworm (Eisenia fetida). J. Soils Sediments 16, 2439–2448.

Kizito, S., Luo, H., Wu, S., Ajmal, Z., Lv, T., Dong, R., 2017. Phosphate recovery from liquid fraction of anaerobic digestate using four slow pyrolyzed biochars: Dynamics of adsorption, desorption and regeneration. J. Environ. Manage. 201, 260–267.

Kizito, S., Lv, T., Wu, S., Ajmal, Z., Luo, H., Dong, R., 2017. Treatment of anaerobic digested effluent in biochar-packed vertical flow constructed wetland columns: Role of media and tidal operation. Sci. Total. Environ 592, 197–205.

Klimmek, S., Stan, H.J., Wilke, A., Bunke, G., Buchholz, R., 2001. Comparative analysis of the biosorption of cadmium, lead, nickel, and zinc by algae. Environ. Sci. Technol. 35, 4283–4288.

Kosik, P.K., Bo, P., Yong, S.O., Mohan, D., Oleszczuk, P., 2020. Engineered biochar - a sustainable solution for the removal of antibiotics from water. Chem. Eng. J.

Kumar, H., Sarswat, A., Alexandre-Franco, M., Pittman, C.U., 2014. Cadmium and lead remediation using magnetic oak wood and oak bark fast pyrolysis bio-chars. Chem. Eng. J.

Kumarathilaka, P., Seneweera, S., Meharg, A., Bundschuh, J., 2018. Arsenic speciation dynamics in paddy rice soil-water environment: sources, physico-chemical, and biological factors-a review. Water Res. 140.

Langmuir, I., 1918. The adsorption of Gases and liquid on plane surfaces of glass, mice and platinum. J. Am. Chem. Soc. 40, 1361–1403.

Li, W., Sohail, M., Anwar, U., Taha, T.A., Al-Sehemi, A.G., Muhammad, S., Al-Ghamdi, A.A., Amin, M.A., Palamanit, A., Ullah, S., Hayat, A., Ajmal, Z., 2022. Recent progress in g–C₃N₄–based materials for remarkable photocatalytic sustainable energy. Int. J. Hydrogen Energy 47, 21067–21118.

Luo, H.H., Liu, L.K., Zhu, D.P., Chang-Lun, X.U., Tang, Y.Y., Zhang, Z.Y., 2017. Research process in removing magnesium and manganese from huangmailing phosphorite mine. China Non-Metal. Miner. Industry.

Luo, X., Wang, C., Luo, S., Dong, R., Tu, X., Zeng, G., 2012. Adsorption of As (III) and As (V) from water using magnetite Fe3O4-reduced graphite oxide-MnO2 nanocomposites. Chem. Eng. J. -LAUSANNE- 187, 45–52.

Malik, A., Hussain, M., Uddin, F., Raza, W., Hussain, S., Habiba, U.-E., Malik, T., Ajmal, Z., 2021. Investigation of textile dyeing effluent using activated sludge system to assess the removal efficiency. Water Environ. Res. 93, 2931–2940.

Meng, S., Meng, X., Fan, W., Liang, D., Wang, L., Zhang, W., Liu, Y., 2020. The role of transparent exopolymer particles (TEP) in membrane fouling: a critical review. Water. Res. 181, 115930.

Min, J., Min, S.H., Kim, T.H., Park, J.K., 2006. Removal of arsenite and arsenate using hydrous ferric oxide incorporated into naturally occurring porous diatomite. Environ. Sci. Technol. 40, 1636.

Mudhoo, A., Sharma, S.K., Garg, V.K., Tseng, C.H., 2011. Arsenic: an overview of applications, health, and environmental concerns and removal processes. Crit. Rev. Environ. Sci. Technol. 41.

Naciri, Y., Chennah, A., Jaramillo-Páez, C., Navío, J., Bakiz, B., Taoufyq, A., Ezahri, M., Villain, S., Guinneton, F., Benlhachem, A., 2019. Preparation, characterization and photocatalytic degradation of Rhodamine B dye over a novel Zn₃(PO₄)₂/BiPO₄ catalyst, Journal of Environmental. Chem. Eng.

Naiya, T.K., Bhattacharya, A.K., Das, S.K., 2009. Adsorption of Cd (II) and Pb(II) from aqueous solutions on activated alumina. J. Colloid Interface Sci. 333, 14–26.

Nassar, N.N., 2010. Rapid removal and recovery of Pb(II) from wastewater by magnetic nanoadsorbents. J. Hazard. Mater. 184, 538–546.

Navarathna, C.M., Karunanayake, A.G., Gunatilake, S.R., Pittman, C.U., Mlsna, T., 2019. Removal of Arsenic(III) from water using magnetite precipitated onto Douglas fir biochar. J. Environ. Manage. 250, 109429.

Ngah, W.S.W., Endud, C.S., Mayanar, R., 2002. Removal of copper (II) ions from aqueous solution onto chitosan and cross-linked chitosan beads. React. Funct. Polym. 50, 181–190.

Pan, F., Sohail, M., Taha, T.A., Al-Sehemi, A.G., Ullah, S., AlSalem, H.S., Mersal, G.A.M., Ibrahim, M.M., Alenad, A.M., Al-Hartomy, O.A., Amin, M.A., Ajmal, Z., Palamanit, A., Hayat, A., Zada, A., Nawawi, W.I., 2022. A facile molecular aggregation of isoquinoline based g-C₃N₄ for high photocatalytic performance under visible light illumination. Mater. Res. Bull. 152, 111865.

Perlman, J.H., Nussenzveig, D.R., Osman, R., Gershengorn, M.C., 267 (1992).. Thyrotropin-releasing hormone binding to the mouse pituitary receptor does not involve ionic interactions. a model for neutral peptide binding to G protein-coupled receptors. J. Biol. Chem. 267.

Qadeer, A., Saqib, Z.A., Ajmal, Z., Xing, C., Khan Khalil, S., Usman, M., Huang, Y., Bashir, S., Ahmad, Z., Ahmed, S., Thebo, K.H., Liu, M., 2020. Concentrations, pollution indices and health risk assessment of heavy metals in road dust from two urbanized cities of Pakistan: comparing two sampling methods for heavy metals concentration. Sustain. Cities. Soc. 53, 101959.

Qadeer, A., Ajmal, Z., Usman, M., Zhao, X., Chang, S., 175 (2021). Agricultural plastic mulching as a potential key source of microplastic pollution in the terrestrial ecosystem and consequences. Resour., Conserv. Recycl. 175, 105855.

Qadeer, A., Kirsten, K.L., Ajmal, Z., Xingru, Z., 2022. Rebuttal to comment on "alternative plasticizers as emerging global environmental and health threat: another regrettable substitution?" focus on DINCH as an example. Environ. Sci. Technol. 56, 5294–5297.

Qadeer, A., Kirsten, K.L., Ajmal, Z., Jiang, X., Zhao, X., 2022. Alternative plasticizers as emerging global environmental and health threat: another regrettable substitution? Environ. Sci. Technol. 56, 1482–1488.

Safa, Y., Bhatti, H.N., 2011. Kinetic and thermodynamic modeling for the removal of Direct Red-31 and Direct Orange-26 dyes from aqueous solutions by rice husk. Desalination 272, 313–322.

Shakoor, M.B., Niazi, N.K., Bibi, I., Murtaza, G., Ali, F., 2016. Remediation of arsenic-contaminated water using agricultural wastes as biosorbents. Crit. Rev. Environ. Sci. Technol. 46.

Tan, X., Liu, Y., Zeng, G., Wang, X., Hu, X., Gu, Y., Yang, Z., 2015. Application of biochar for the removal of pollutants from aqueous solutions. Chemosphere 125, 70–85.

Tang, Y., Zhang, X.Y., Wang, Q.P., Wang, W.T., Wu, Z.G., Li, L., Zhang, X.L., Zhang, Y.G., Liu, Z.J., Chen, X.H., 2011. High-efficiency diode-pumped acousto-optically Q-switched 1123 nm ceramic Nd:YAG laser. Laser Phys. 21, 695–699.

Tofan, L., Wenkert, R., Paduraru, C., 2016. Natural and waste materials as green sorbents for cd(ii) removal from aqueous effluents. Environ. Eng. Manage. J. 15, 1049–1058.

Tuutijärvi, T., Repo, E., Vahala, R., Sillanpää, M., Chen, G., 2012. Effect of competing anions on arsenate adsorption onto maghemite nanoparticle. Chin. J. Chem. Eng.

Urík, M., Littera, P., Ševc, J., Kolenčík, M., Čerňanský, S., 2009. Removal of arsenic (V) from aqueous solutions using chemically modified sawdust of spruce (Picea abies): Kinetics and isotherm studies. Int. J. Environ. Sci. Technol. 6.

Usman, M., Bd Elmoula, M.A., Hanna, K., Grégoire, B., Faure, P., Ruby, C., 2012. FeII induced mineralogical transformations of ferric oxyhydroxides into magnetite of variable stoichiometry and morphology. J. Solid State Chem. 194, 328–335.

Usman, M., Faure, P., Lorgeoux, C., Ruby, C., Hanna, K., 2013. Treatment of hydrocarbon contamination under flow through conditions by using magnetite catalyzed chemical oxidation. Environ. Sci. Pollut. Res. 20, 22–30.

Usman, M., Byrne, J.M., Chaudhary, A., Orsetti, S., Haderlein, S.B., 2018. Magnetite and green rust: synthesis, properties, and environmental applications of mixed-valent iron minerals. Chem. Rev. 118, 3251–3304.

Vatutsina, O.M., Soldatov, V.S., Sokolova, V.I., Johann, J., Bissen, M., Weissenbacher, A., 2007. A new hybrid (polymer/inorganic) fibrous sorbent for arsenic removal from drinking water. React. Funct. Polym. 67, 184–201.

Wan, Z., Cho, D.-W., Tsang, D.C., Li, M., Sun, T., Verpoort, F., 2019. Concurrent adsorption and micro-electrolysis of Cr (VI) by nanoscale zerovalent iron/biochar/Ca-alginate composite. Environ. Pollut. 247, 410–420.

Wang, S., Bian, S., Liu, J., Li, J., Xu, S., Liang, Z., 2021. Highly adsorptive pristine and magnetic biochars prepared from crayfish shell for removal of Cu (II) and Pb (II). J. Taiwan Inst. Chem. Eng. 127, 175–185.

Wang, J.T., Chuang, Y.C., Chen, K.L., Lu, C.C., Doong, S.L., Cheng, H.H., Chen, Y.L., Liu, T.Y., Chang, Y., Han, C.H., 2010. Characterization of Epstein-Barr virus BGLF4 kinase expression control at the transcriptional and translational levels. J. Gen. Virol. 91, 2186–2196.

Wang, Z., Guo, H., Shen, F., Yang, G., Zhang, Y., Zeng, Y., Wang, L., Xiao, H., Deng, S., 2015. Biochar produced from oak sawdust by Lanthanum (La)-involved pyrolysis for adsorption of ammonium (NH4+), nitrate (NO3), and phosphate (PO43). Chemosphere 119, 646–653.

Wei, L., Chen, D., Fang, X., Tan, J., Huang, P.P., Song, W.G., Nursam, N.M., Caruso, R.A., 2016. Extremely high arsenic removal capacity for mesoporous aluminium magnesium oxide composites. Environ. Sci. Nano 3.

Wu, S., Lv, T., Lu, Q., Ajmal, Z., Dong, R., 2017. Treatment of anaerobic digestate supernatant in microbial fuel cell coupled constructed wetlands: Evaluation of nitrogen removal, electricity generation, and bacterial community response. Sci. Total Environ. 580, 339–346.

Xi, J., Wang, Q., Duan, X., Zhang, N., Yu, J., Sun, H., Wang, S., 2021. Continuous flow reduction of organic dyes over Pd-Fe alloy based fibrous catalyst in a fixed-bed system. Chem. Eng. Sci. 231, 116303.

Xiong, C., Wang, W., Tan, F., Luo, F., Qiao, X., 2015. Investigation on the efficiency and mechanism of Cd(II) and Pb(II) removal from aqueous solutions using MgO nanoparticles. J. Hazard. Mater. 299, 664–674.

Yin, W., Zhang, W., Zhao, C., Xu, J., 2019. Evaluation of Removal Efficiency of Ni(II) and 2,4-DCP Using in Situ Nitrogen-Doped Biochar Modified with Aquatic Animal Waste. ACS Omega, XXXX.

Ying, A., Zhang, Q., Li, H., Shen, G., Gong, W., He, M., 2013. An environmentally benign protocol: catalyst-free Michael addition of aromatic amines to α, β-unsaturated ketones in glycerol. Res. Chem. Intermed. 39, 517–525.

A. Yn, A. Ah, B. Za, C. Aba, A. Bb, D. Jan, A. Aa, C. Jcv, A. Me, A. Ab, Influence of Sr-doping on structural, optical and photocatalytic properties of synthesized $Ca_3(PO_4)_2$, Journal of colloid and interface science, 572 269-280.

Yoo, P., Amano, Y., Machida, M., 2018. Adsorption of nitrate onto nitrogen-doped activated carbon fibers prepared by chemical vapor deposition. Korean J. Chem. Eng. 35, 2468–2473.

W. Yu, F. Lian, G. Cui, Z. Liu, accepted manuscript n-doping effectively enhances the adsorption capacity of biochar for heavy metal ions from aqueous solution n-doping effectively enhances the adsorption capacity of biochar for heavy metal 1 ions from aqueous solution 2 3.

Zhang, W., Jiang, F., 2019. Membrane fouling in aerobic granular sludge (AGS)-membrane bioreactor (MBR): effect of AGS size. Water Res. 157, 445–453.

Zhang, W., Liang, W., Zhang, Z., Hao, T., 2021. Aerobic granular sludge (AGS) scouring to mitigate membrane fouling: performance, hydrodynamic mechanism and contribution quantification model. Water Res. 188, 116518.

Zhang, N., Qiu, Y., Sun, H., Hao, J., Chen, J., Xi, J., Liu, J., He, B., Bai, Z.-W., 2021. Substrate-assisted encapsulation of Pd-Fe bimetal nanoparticles on functionalized silica nanotubes for catalytic hydrogenation of nitroarenes and azo dyes. ACS Appl. Nano Mater. 4, 5854–5863.

Zhang, L., Zhu, T., Liu, X., Zhang, W., 2016. Simultaneous oxidation and adsorption of As(III) from water by cerium modified chitosan ultrafine nanobiosorbent. J. Hazard. Mater. 308, 1–10.

Zhang, Liankai, Yang, Hui, Tang, Jiansheng, Qin, Xiaoqun, Liu, Wen, Review of arsenic geochemical characteristics and its significance on arsenic pollution studies in karst groundwater, Southwest China, Applied Geochemistry: Journal of the International Association of Geochemistry and Cosmochemistry, 77 (2017) 80-88

Zhu, L.P., Liao, G.H., Yang, Y., Xiao, H.M., Fu, W., 2009. Self-assembled 3D flower-like hierarchical β-Ni(OH)₂ hollow architectures and their in situ thermal conversion to NiO. Nanoscale Res. Lett.